Structures 33 (2021) 4596–4603

Contents lists available at ScienceDirect

Structures

journal homepage: www.elsevier.com/locate/structures

A precise time-integration linear vehicle-bridge interaction method and dynamic sensitivity analysis

Yuefeng Shao [a,b,c,*], J.M.W. Brownjohn [c], Changqing Miao [a,b,*], Miaomin Wang [c,d]

[a] Key Laboratory of Concrete and Prestressed Concrete Structures of Ministry of Education, Southeast University, Nanjing, PR China
[b] School of Civil Engineering, Southeast University, Nanjing 211189, PR China
[c] Vibration Engineering Section, College of Engineering, Mathematics and Physical Sciences, University of Exeter, North Park Road, EX4 4QF Exeter, United Kingdom
[d] School of Civil Engineering, Dalian University of Technology, Dalian 116024, PR China

ARTICLE INFO

Keywords:
Vehicle-bridge interaction
Linear dynamic
Precise time-integration method
Modal superposition technique
Half-vehicle model
Full-vehicle model

ABSTRACT

A linear dynamic vehicle-bridge interaction method is proposed in this paper. This VBI system can be easily simulated by a step-by-step solution technique based on precise time-integration method following discretization of the bridge and modal analysis of the finite element model. By selecting the target structural mode with high modal participation in finite element modal analysis, the huge computational overhead caused by the multi-degrees of freedom of large structures in the dynamic response analysis can be effectively reduced. In this integration process, the characteristics of precise time-integration method can be used to ensure the stability and accuracy of the iterative calculation when selecting a relatively large time integration step. This provides the possibility to investigate the VBI problem in large-scale bridges. In this work, a half-vehicle model case and an experiment on full-vehicle model are used to verify the application of the algorithm. Then the dynamic sensitivity of a beam is analyzed based on the dynamic amplification factor.

1. Introduction

Vehicle-induced vibration is one of the primary concerns in bridge design and assessment, in which the dynamic amplification factor (DAF) [1], which is generally based on the maximum dynamic and static responses, is an important evaluation parameter. However, the evaluation of DAF is a rather complicated issue because of the sophisticated mechanism of the vehicle-bridge interaction (VBI) [2].

To solve the VBI problem, monitoring of the real bridge [3–5] can directly obtain the dynamic response data of a real bridge. But it requires significant capital investment and requires appropriate denoising methods [6,7] to filter the useful data. The damage state of bridges can also be detected by some economy ways [8,9]. However, the dynamic performance of highway bridges cannot be monitored by those real-time methods under complex traffic conditions. The research on numerical analysis methods [10,11] of bridge vibration response has been continuously developed due to its economic efficiency.

In early VBI numerical dynamic studies, analytical methodologies were proposed to analyze behavior of the idealized simply-supported beam (SSB) in the presence of dynamic loads, such as a moving mass or force [12]. The application of finite element modeling (FEM) extended the range of candidates for numerical analysis from SSB structures to realistic bridges in VBI dynamic studies [13,14]. However, simulation of dynamic response of realistic bridge structures by FEM may involve a huge computational overhead.

In such dynamic analysis, integration schemes, such as Newmark-β and Wilson-θ methods [15,16], can be made unconditionally stable by proper selection of the integration parameters. Choice of integration time step in implicit integration is problematic since high frequency components in vibration will be distorted when taking a large time step value [17], while choosing a small value will require greater computational effort.

To avoid such difficulties, a linear VBI dynamic analysis system based on modal decomposition and precise time step integration theory is proposed. In this system, the bridge is replaced by selected modal components, according to evaluation of modal participation factor. And the implicit integration of dynamic analysis can maintain the accuracy while taking a relatively larger time interval, due to the 2^N algorithm within the time step size [17]. Then the dynamic sensitive area of structure can be evaluated based on the dynamic response obtained by this optimized VBI system.

The outline of the paper is as follows: Section 2 presents the theory of

* Corresponding authors at: Key Laboratory of Concrete and Prestressed Concrete Structures of Ministry of Education, Southeast University, Nanjing, PR China.
E-mail addresses: Y.Shao@exeter.ac.uk (Y. Shao), chqmiao@163.com (C. Miao).

https://doi.org/10.1016/j.istruc.2021.07.025
Received 6 May 2021; Received in revised form 30 June 2021; Accepted 6 July 2021
Available online 23 July 2021

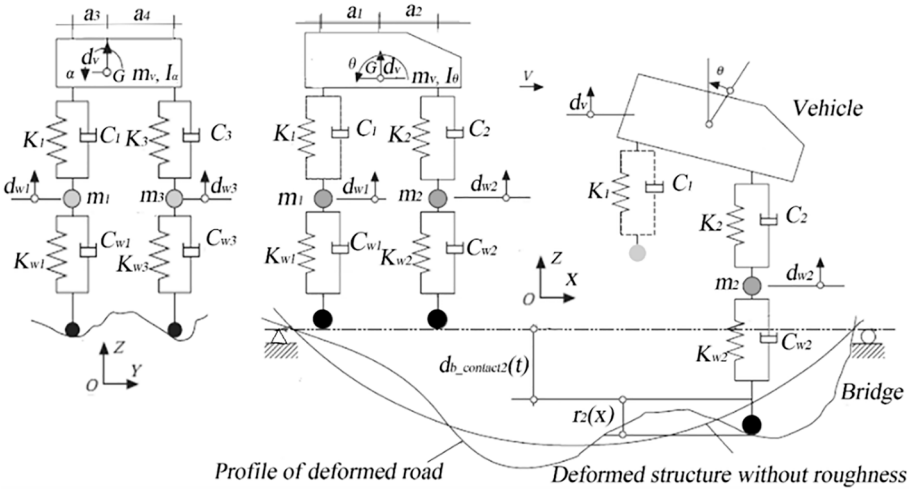

Fig. 1. Vehicle model with 7-DOFs and bridge-vehicle interaction.

dynamic VBI based on FEM bridge structure modeling. In section 3, a half-vehicle dynamic case and a full-vehicle model dynamic experiment is presented to verify the VBI system. Finally, section 4 presents the dynamic sensitive area analysis of the beam through the proposed VBI system.

2. Moving mass on bridge linear dynamic analysis

2.1. Modalized bridge model

Modal superposition in FEM is an effective means to reduce the computation in linear dynamic analysis of complex structures. This section presents the approach for modal masses corresponding to unity-scaled mode shapes i.e. where mode shape translation ordinates for translation are set to absolute value 1.0 [18].

For vertical harmonic displacement at node *i* for mode *r*, the 'unity scaled' modal mass is obtained from the maximum amplitude of a mass normalized mode shape element (DMX_r) [19].

$$\{\phi_{i,r}\}^T[M_b]\{\phi_{i,r}\} = \frac{1}{DMX_r^2} \tag{1}$$

where $[M_b]$ is the bridge structural matrices of mass.$\{\phi_{i,r}\}$ is r^{th} unity scaling mode shape of the bridge at node *i*.

The structural stiffness matrix $[K_b]$ is equal to $\overline{\omega}_r^2[M_b]$, and the damping matrix $[C_b]$ is assumed to be equal to $\alpha[M_b] + \beta[K_b]$, where α and β are the Rayleigh damping coefficients. The single degree of freedom dynamic equations for the bridge FEM are:

$$\frac{1}{DMX_r^2}\left[\left\{\ddot{\xi}_b\right\} + \left(\alpha + \beta\overline{\omega}_r^2\right)\left\{\dot{\xi}_b\right\} + \overline{\omega}_r^2\{\xi_b\}\right] = \left[\phi_{i,r}\right]^T\{F_b\} \tag{2}$$

where $\left\{\ddot{\xi}_b\right\},\left\{\dot{\xi}_b\right\},\{\xi_b\}$ are the bridge normal coordinates [20] corresponding acceleration, velocity and displacement vector, $\{F_b\}$ is forces vector of the bridge.

2.2. VBI system and vehicle model

The VBI system and vehicle model are presented in Fig. 1. The vehicle motion equation is shown as follows [21–23]:

$$[M_v]\cdot\left\{\ddot{d}_v\right\} + [C_v]\cdot\left\{\dot{d}_v\right\} + [K_v]\cdot\{d_v\} = -\{F_G\} + \{F_{v-b}\} \tag{3}$$

where $[M_v],[C_v],[K_v]$ are the mass matrices, damping matrices and stiffness matrices of vehicle, respectively, $\left\{\ddot{d}_v\right\}$, $\left\{\dot{d}_v\right\}$, $\{d_v\}$ are the vertical acceleration, velocity and displacement vector of vehicle, $\{F_G\}$ is the gravity load of vehicle, and $\{F_{v\text{-}b}\}$ is the interaction force between the bridge and vehicle.

A 7- degree of freedoms (7-DOFs) vehicle model was taken as an example (as shown in Fig. 1). 7-DOFs involve vehicle body bounce, pitch, roll and 4-wheel vertical motions. K_j and C_j are the stiffness and damping of vehicle body suspension; K_{wj} and C_{wj} are the wheel stiffness and damping; m_v and m_i are the mass of vehicle body and wheels, respectively. (j = 1,2,3,4). a_1 and a_2 are the distance of rear and front wheels to barycenter of vehicle. $a3$ and $a4$ are the distance between wheels and vehicle barycenter.

When a vehicle is present on the bridge, the interaction force between j^{th} wheel and bridge is shown as follows:

$$F_{v-b}^j = -F_{b-v}^j = -K_{wj}\cdot\Delta_j - C_{wj}\cdot\dot{\Delta}_j \quad (j = 1,2,3\ldots) \tag{4}$$

$$\Delta_j = d_{wj} - d_{b\_contactj} - r_j(x), \quad \dot{\Delta}_j = \dot{d}_{wj} - \dot{d}_{b\_contactj} - \dot{r}_j(x) \tag{5}$$

where Δ_j and $\dot{\Delta}_j$ are, respectively, the relative vertical displacement and velocity between the j^{th} wheels and bridge, $r_j(x)$ road surface roughness under j^{th} wheels.

Based on the FEM theory, $d_{b\_contact}$ can be obtained by using the bridge shape function equation at j^{th} vehicle wheels, and node displacement of the bridge $\{d_b\}$.

$$d_{b\_contactj} = \left[N_b^j\right]\cdot\{d_b\} \tag{6}$$

2.3. Modal selection based on modal correlation factor

The steady state dynamic response analysis of real-world multi-DOF structures is always computationally very costly. This study employs linear modes of the structure to reduce the amount of calculation. In order to select the appropriate number of modes for dynamic analysis, the modal correlation ratio [24,25], which represents the contribution to the structure dynamic response, is introduced. The representative values for the modal response are defined as the modal participation in structural deflection (MPS) and modal participation in node deflection (MPN), which can quantitatively represent the contribution of a particular vertical mode to structural dynamic response. They are calculated as follows:

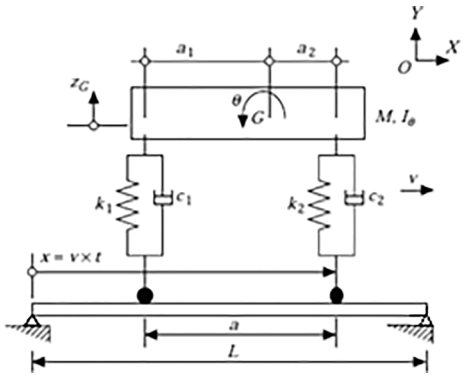

Fig. 2. Half-vehicle analysis system [29].

Table 1
Parameters of SSB and half-vehicle [29].

Beam parameters	Vehicle parameters
$L = 1.1938$ m	$M_v = 4.4025$ kg
$\rho = 2.9602 \times 10^3$ kg/m^3	$I_\theta = 0.56825$ kg m^2/rad
$A = 0.51 \times 10^{-2}$ m^2	$K_1 = 2.164 \times 10^{-2}$N/m
$I = 0.9448 \times 10^{-5}$ m^4	$K_2 = 1.803 \times 10^{-2}$N/m
$E = 10.48 \times 10^{10}$N/m^2	$C_1 = C_2 = 0$
(Modal damping ratio) $\zeta_1 = \zeta_2 = 0$	$a_1 = 0.348$ m, $a_2 = 0.371$ m

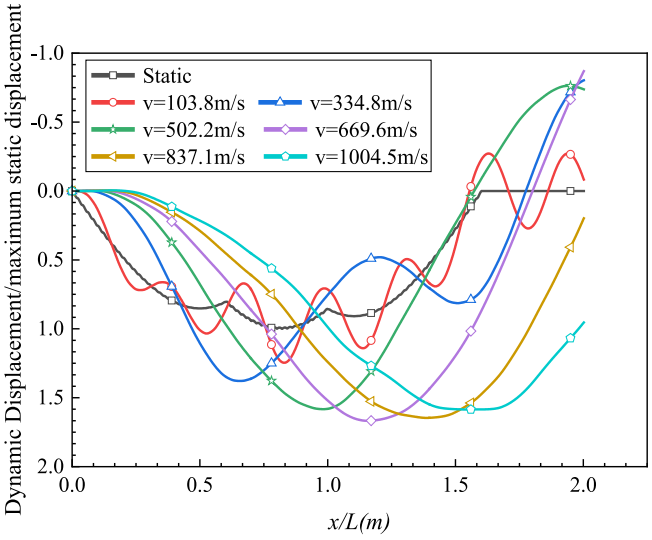

Fig. 3. The central dynamic deflection of SSB.

Table 2
The damping parameters of the simply-supported beam and vehicle model.

	Case 1		Case 2	
Simply-supported beam	$\zeta_1 = 0$	$\zeta_2 = 0$	$\zeta_1 = 0.02$	$\zeta_2 = 0.05$
Vehicle model	$c_1 = 0$	$c_2 = 0$	$c_1 = 88.68$ N s/m	$c_2 = 78.41$ N s/m

Table 3
DAF of the simply-supported beam.

	Case 1		Case 2	
v(m/s)	VBI system	Reference[29]	VBI system	Reference[29]
103.8	1.246	1.246	1.154	1.173
334.8	1.378	1.381	1.305	1.342
502.2	1.583	1.582	1.490	1.535
669.6	1.667	1.665	1.567	1.616
837.1	1.646	1.651	1.545	1.601
1004.5	1.585	1.590	1.495	1.550

Fig. 4. OPAL^{TM} IMUs.

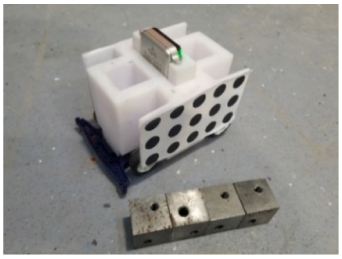

Fig. 5. The vehicle with weight and OPAL.

$$MPS_r = \frac{\sum_{i=1}^{n_d} \sqrt{\sum_{k=1}^{n_t} z_r^i(k)^2 / n_t}}{\sum_{r=1}^{n_m} \sum_{i=1}^{n_d} \sqrt{\sum_{k=1}^{n_t} z_r^i(k)^2 / n_t}} \quad r = 1 \text{ to } n_m,\ i = 1 \text{ to } n_d \tag{7}$$

$$MPN_r = \frac{\sqrt{\sum_{k=1}^{n_t} z_r^i(k)^2 / n_t}}{\sum_{i=n_{lb}}^{n_{le}} \sum_{r=1}^{n_m} \sqrt{\sum_{k=1}^{n_t} z_r^i(k)^2 / n_t}} \quad r = 1 \text{ to } n_m,\ i = n_{lb} \text{ to } n_{le} \tag{8}$$

where z_r^i is the vertical modal displacement at structural node i for mode r. n_t is total number of time-steps, n_m is the number of selected modes, n_d is number of structural nodes. k is the time step. n_{lb} and n_{le} are node number of a selected part in the structure.

2.4. Multi-DOFs structure dynamic solution: precise integration method (PIM)

The set of ordinary differential equations Eq. (2) can be transformed to state space as [17]

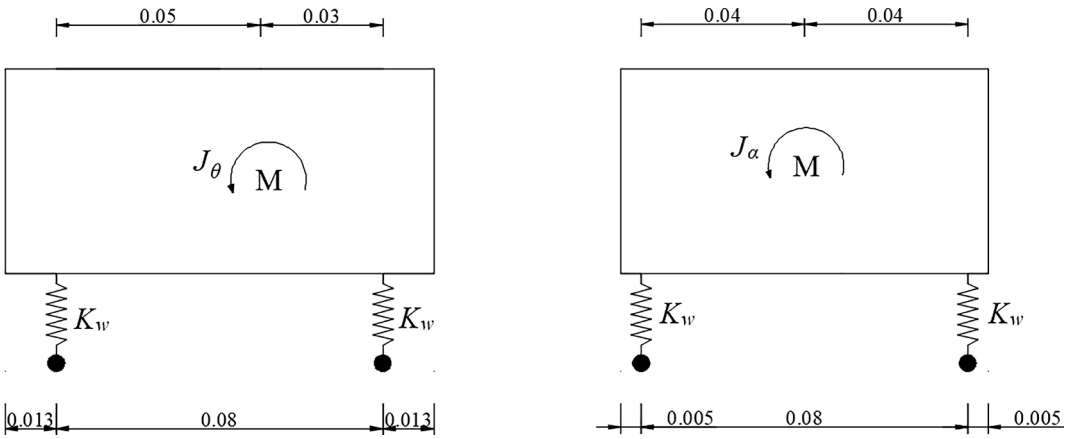

Fig. 6. Full-vehicle model with 3-DOFs (m).

Table 4
The vehicle Parameter.

First 3 natural frequencies of vehicle	Measured (Hz)	Simplified model (Hz)
$f1$	8.75	8.65
$f2$	21.87	21.90
$f3$	30.62	29.87
Empty vehicle quality	0.288 kg	
Quality of counterweight	0.1016 kg × 4	
J_θ	0.0002 kg·m^2	
J_α	0.0001 kg·m^2	
K_w	550.48 N/m	

$$\dot{v} = Hv + f;\quad H = \begin{bmatrix} -\frac{\alpha+\beta\overline{\omega}_r^2}{2} & DMX_r^2 \\ \frac{1}{DMX_r^2}\left(\frac{\left(\alpha+\beta\overline{\omega}_r^2\right)^2}{4} - \overline{\omega}_r^2\right) & -\frac{\alpha+\beta\overline{\omega}_r^2}{2} \end{bmatrix};$$

$$f = \begin{Bmatrix} 0 \\ [\phi_r]^T\{F_b\} \end{Bmatrix};\quad v = \begin{Bmatrix} \{\xi_b\} \\ \frac{1}{DMX_r^2}\left(\left\{\dot{\xi}_b\right\} + \frac{\left(\alpha+\beta\overline{\omega}_r^2\right)}{2}\{\xi_b\}\right) \end{Bmatrix} \tag{9}$$

Based on the algorithm of PIM [26–28], the inhomogeneous Eq. (9) can be solved by the superposition principle as

$$v_{k+1} = exp(H\times\Delta t)\times\left[v_k + H^{-1}(f(t_k)+H^{-1})\right] - H^{-1}\left[f(t_k) + H^{-1}\Delta f + \Delta t\Delta f\right]$$
$$\Delta f = f(t_{k+1}) - f(t_k) \tag{10}$$

3. Validation of the VBI method

3.1. VBI solution under half-vehicle model

Half-vehicle model is a classic loading model applied in the analysis of VBI. To validate this VBI method in the application of half-vehicle model loading, a simply-supported beam (SSB) dynamic response analysis, which has been applied in reference [22,29], is performed as shown in Fig. 2. Dividing the structure into 20 beam4 elements for modal analysis in ANSYS. In VBI analysis, the gravity acceleration is 9.8 m/s^2, and the other parameters of SSB and vehicle are shown in Table 1. The beam dynamic VBI solutions under the loading state of 6 different vehicle velocities are shown in Fig. 3.

The dynamic response of the beam and vehicle body obtained by VBI method agree well with the validated analysis in reference [22,29], which further confirms the reliability and accuracy of proposed method in the dynamic analysis of half-vehicle model and beam interaction. For example, Fig. 3 shows the central dynamic deflection of SSB loaded by half-vehicle at different speeds. They are agreed well with the dynamic deflection curves obtained from reference [22,29].

When considering the influence of damping (the damping parameters are shown in Table 2), the dynamic amplification factor (DAF) of this beam at different velocities are shown in Table 3.

As shown in Table 3, the DAFs agree well with those found in reference [29]. There is a significant correlation between beam's

Table 5
Material properties and element selection of FEM beam.

Elastic Modulus	Poisson's Ratio	Mass Density	Element
2.06*10^{11}N/m^2	0.28	7800 kg/m^3	SHELL63

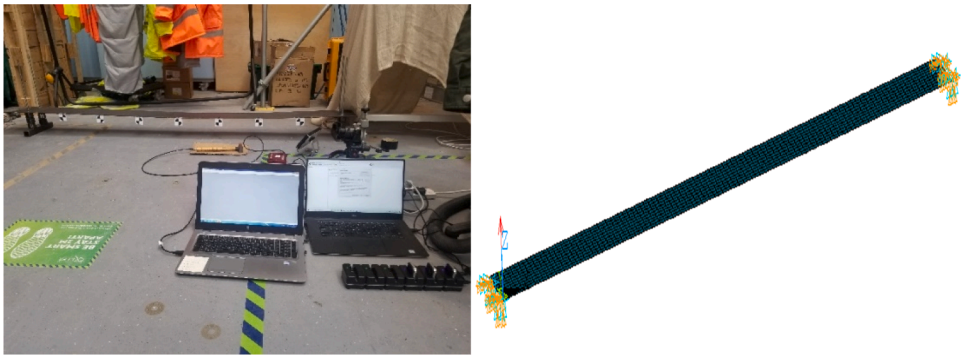

Fig. 7. Beam (left) and its FEM (right).

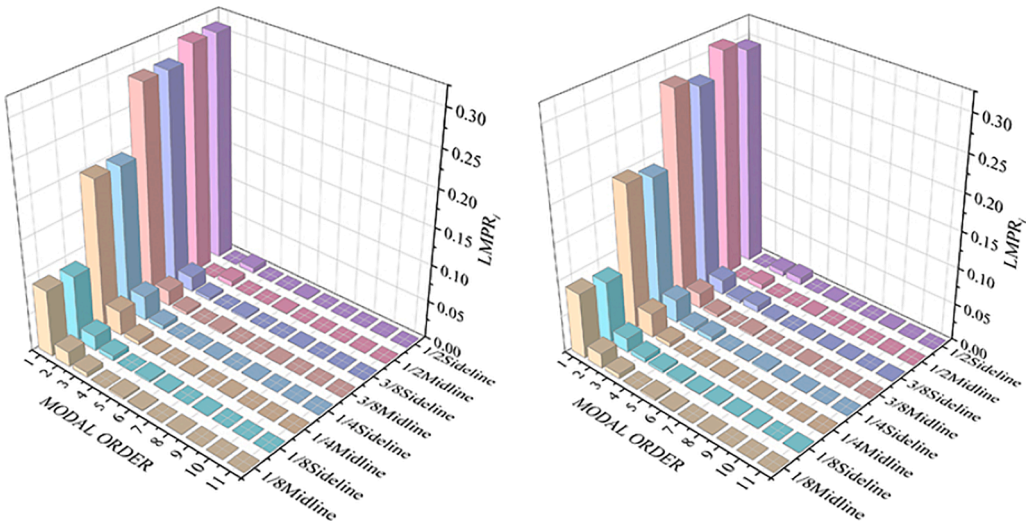

Fig. 8. MPN_i of symmetric loading (left) and eccentric loading (right).

Table 6
Experimental and simulated values of first 3 beam natural frequencies.

Order	Simulation (Hz)	Experiment (Hz)
1	4.33	4.58
2	13.67	13.99
3	29.36	31.86

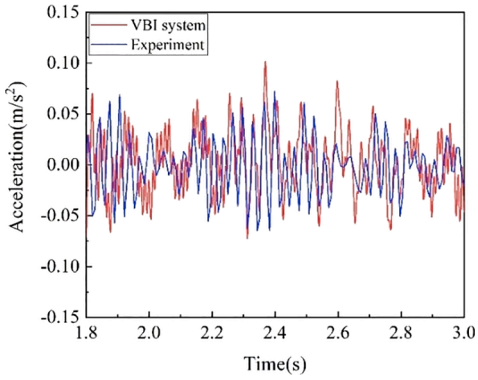

Fig. 9. The mid-span node acceleration time history curve comparison between VBI system and test.

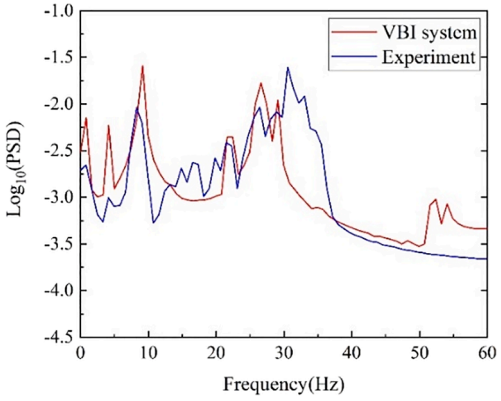

Fig. 10. PSD of acceleration time history.

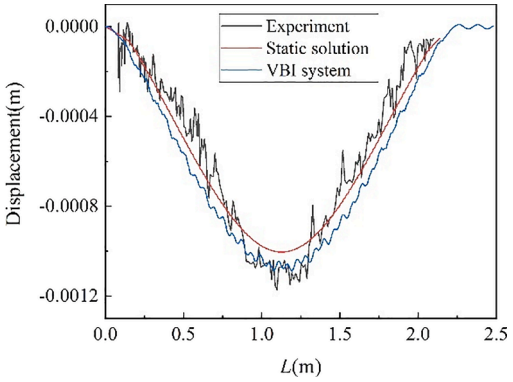

Fig. 11. The mid-span node displacement of test steel beam subjected to different loads.

dynamic response and vehicle velocity. Within a certain velocity range, the vehicle velocity is proportional to dynamic response of beam. When the velocity exceeds the limit value, vehicle velocity is in inverse ratio to dynamic response of beam. The damping of structure and vehicle can also weaken the dynamic effect of the structure. The damping effect changes with the vehicle velocity.

3.2. Experimental procedure for full-vehicle model loading

Many direct or indirect experimental techniques can be used to identify the dynamic behavior of bridge and vehicle [3–5], however, the test result of field work often accompanied by the environmental noise. To avoid this, the dynamic response of a SSB and vehicle were identified by the inertial measurement units (IMUs) in the laboratory. The OPAL^{TM} IMUs (Fig. 4), which are typically used in human biomechanics research [30,31] are used in this research. They were securely fixed to the vehicle and at the 1/2 and 1/4 spans of SSB to obtain the acceleration of vehicle and beam, respectively.

During the loading process, the continuous shape of deflection of the bridge was recorded by a 4 K and 60 frame per second video camera, with the displacement time history of the beam obtained through image processing.

As shown in Fig. 5, the vehicle is powered by two AA batteries. The full-vehicle model with 3-DOF is shown in Fig. 6, and the influence of vehicle damping was ignored in this case. Ignoring the acceleration and deceleration stage of the vehicle due to the beam deflection, the

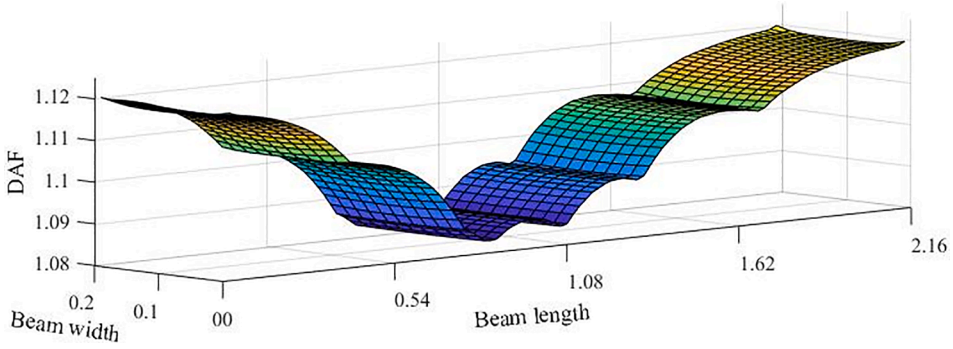

Fig. 12. The DAF of the experimental beam.

Table 7
The maximum dynamic and static displacement in longitudinal direction (mm).

	Dynamic displacement	Static displacement
1/8-span	0.3603	0.3223
1/4-span	0.7275	0.6601
3/8-span	0.9866	0.9110
1/2-span	1.0890	1.0038

measured average speed of the vehicle was 0.5 m/s. The parameter of this moving mass is shown in Table 4.

To examine the VBI system, analysis of a SSB and moving mass dynamic system was performed. The steel beam dimensions are 2.16 m length, 0.2 m width, 0.006 m height (Fig. 7) and both ends were fully fixed (bolted). The material properties and element selection of this FEM beam are shown in the Table 5.

3.3. Model information and modal selection of the beam

Based on modal selection in section 2, the first 50 modes of the beam are studied to identify effective modal, i.e. the n_m in Eq. (7) and Eq. (8) can be set to 50. The MPS and MPN in different effective modes are:

$$MPS = \sum_{i=1}^{n_e} MPN_i \tag{11}$$

where n_e is the number of effective modes.

In this selection, we choose a 7 N vertical external moving load based on the mass of the vehicle in the test. As the result, the beam structure is mainly affected by the first three vertical bending modes. For symmetric loading and eccentric loading, the contributions of the 1st bending mode are 86.5% and 84.1% respectively. The torsional modes, such as the 4th and 7th mode, have negligible contribution under symmetric loading. As the total contributions of the first 11 modes in these two loading conditions exceed 99.5%, the influence of the higher order modes (beyond 11th) is ignored to simplify the calculation.

The first eleven modal responses obtained in the two loading modes are substituted into Eq. (8), and the MPN_i of different loading positions are shown in the Fig. 8.

As shown in the Fig. 8, the torsional modes, such as the 4th torsional mode, show the higher modal correlation in eccentric loading, but have no effect in symmetric loading. The response differences among nodes on the same cross section can be ignored during symmetric loading, while the response is mainly controlled by 1st vertical bending mode and affected by 1st torsion mode during asymmetric loading.

Based on the performance of MPS and MPN_i, this study will consider the first eleven vibration modes in the SSB dynamic response analysis.

3.4. Laboratory and numerical simulations for Full-vehicle model

The natural frequencies of the 3-DOF full-vehicle model are 8.75 Hz, 21.87 Hz and 30.62 Hz respectively, i.e. all are less than 32 Hz. Furthermore, the 32 Hz frequency band contains the first three modes of test beam. According to the modal selection result, the TMCR of first three modes is 98.46% by symmetrical loading. To reduce the influence of measurement error, a lowpass filter with a 32 Hz cutoff was used to process the collected signals. The signals were collected by OPAL with 128 Hz sampling frequency.

The experimental and simulated values of first 3 beam natural frequencies are shown in the Table 6.

The experiment and VBI simulation results for mid-span acceleration in time and frequency domains are shown in Fig. 9 and Fig. 10.

In the test, initial velocity of the vehicle was 0. As the reason of beam deflection due to self-weight, vehicle movement can be divided into three stages: acceleration, moving at a relatively constant speed and deceleration. For direct comparison with the simulation results, the second stage (considering the acceleration, uniform motion and deceleration phases) in the whole process (in Fig. 9) is used.

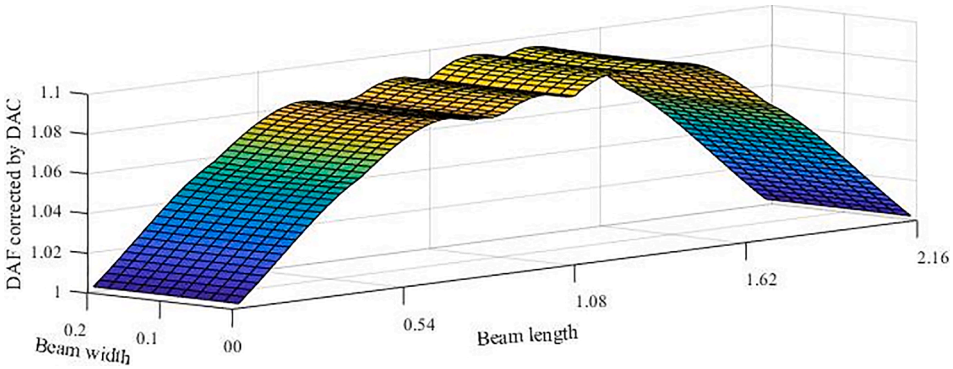

Fig. 13. Corrected DAF of the beam.

The acceleration amplitudes are in good agreement while in frequency domain by FFT (as shown in Fig. 10). Ignoring the errors caused by measurement and acceleration stage selection, the vibration frequency of the beam is mainly composed by the fundamental frequency of the beam (4.15 Hz) and the exciting frequency of the vehicle (8.35 Hz). They are numerically consistent with the natural frequency of the beam and the excitation frequency of the vehicle. Fig. 11 presents the central node displacement of test beam for different loads. The vibration trend of beam displacement roughly agrees.

4. Structure dynamic sensitivity analysis

Although there are several definitions of DAF [2], it is generally based on maximum dynamic and static responses as follows:

$$DAF = 1 + \frac{R_{dyn} - R_{sta}}{R_{sta}} \tag{12}$$

where R_{dyn} and R_{sta} are the maximum dynamic and static response, respectively.

Based on the dynamic and static beam deflection obtained by VBI system, the vertical DAF of the beam is shown in the Fig. 12.

As shown in Fig. 12, since the flexibility in the longitudinal direction of the beam is larger than transverse, nodes on a cross-section of the beam have a similar dynamic amplification characteristic. Due to the relatively small value of static displacement (in Table 7), the small dynamic amplification increments near the support of the beam lead to a relatively large DAF. In spite of the largest dynamic displacement increment at 1/2-span of the beam, DAF value is a minimum because of its large static displacement. Therefore, the DAF cannot clearly present the dynamic sensitive areas distribution of the beam.

In implementing modal superposition to solve for dynamic response to harmonic loading [20], displacement amplitude coefficient (DAC) is used to fix the dynamic sensitive characteristics of DAF. The vehicle load is assumed as a superposition of multiple harmonic loads and is applied to each mode of the structure. Then displacement amplitude of each structure node can be obtained as follows:

$$DA = \sum_{v=1}^{n_v} \sum_{r=1}^{n_m} \frac{MPN_r}{M_r \times \left|\overline{\omega}_r^2 - \omega_v^2\right|} \tag{13}$$

where M_r and $\overline{\omega}_r$ are the r^{th} modal mass and modal frequency of the beam, respectively. ω_v is the v^{th} modal frequency of the vehicle. MPN_r is the modal participation in each node deflection, which is mentioned in section 2.

Under static loading, the maximum displacement amplitude occurs at the mid-span node of the beam. To regard the mid-span node as the reference point and scaling its DA to 1.0, the DAC of i^{th} node can be obtained as follows:

$$DAC_i = DA_i \times \frac{1}{DA_{mid-span}} \tag{14}$$

With the DAC correction, vertical DAF of the beam (Fig. 13) shows an obvious beam dynamic performance between 1/4-span to 3/4 span, where the DAF value fluctuates between 1.08 and 1.1. The maximum DAF appears near the 5/8-span of the beam mainly because the amplitude of the first-order antisymmetric vertical bending mode of the beam in the mid-span is 0, and the maximum static displacement at this area is relatively low, because the rear wheels of the vehicle model carry more weight. Therefore, for a moving vehicle load having fundamental frequency is 8.65 Hz, the dynamic sensitive area of the SSB is between 1/4 span and 3/4 span. The max DAF is 1.095, which is near the 3/4 span.

Under this vehicle excitation, the peak point of beam DAF agrees with the first two vibration mode shapes of the beam, which are the first symmetric vertical bending (4.33 Hz) and first antisymmetric vertical bending (13.67 Hz). The dynamic sensitive area of structure is influenced by the structural mode shapes whose frequencies are close to the frequency of dynamic excitation.

5. Conclusion

A new dynamic method for vehicle-bridge interaction analysis has been proposed. Satisfactory dynamic response can be obtained in the vehicle-bridge interaction analysis of the half-vehicle model and the full-vehicle model. This method optimizes the multi-DOFs structure through modal decomposition, and simultaneously optimizes the integration process by precise time-integration method. Thus, it can be applied to the vehicle-bridge interaction analysis of large-scale bridges after considering road surface roughness.

Based on the displacement amplitude coefficient (DAC) at different part of the bridge, the dynamic amplification factor is corrected, which can show the dynamic sensitive area of the bridge more clearly. It is influenced by the mode shape of the structure whose frequency is close to the excitation frequency. For example, the dynamically more sensitive area of the SSB simulated in this paper can be located between 1/4-span to 3/4 span. The first symmetric vertical bending mode and the first antisymmetric vertical bending mode have high influence on the dynamic sensitive area.

Declaration of Competing Interest

The authors declare that they have no known competing financial interests or personal relationships that could have appeared to influence the work reported in this paper.

Acknowledgments

This paper was supported by National Natural Science Foundation of China (Grant Number 51778135), the Distinguished Young Scientists of Jiangsu Province (Grant Number BK20190013). Authors thank Steve Hubbard, Dr. Waikei Ao and Karen Faulkner for providing assisting with beam-vehicle dynamic experiment at University of Exeter and thank Dr. Huiyi Yang and Olivia Zhang for providing assisting with paper reviewing.

References

[1] Paultre P, Chaallal O, Proulx J. Bridge dynamics and dynamic amplification factors—a review of analytical and experimental findings. Can J Civ Eng 1992;19(2):260–78.
[2] Deng L, Yu Y, Zou Q, Cai CS. State-of-the-art review of dynamic impact factors of highway bridges. J Bridge Eng 2015;20(5):04014080. https://doi.org/10.1061/(ASCE)BE.1943-5592.0000672.
[3] Hester D, González A. A bridge-monitoring tool based on bridge and vehicle accelerations. Struct Infrastruct Eng 2015;11(5):619–37.
[4] Vardanega P J, Webb G T, Fidler P R, et al. Assessing the potential value of bridge monitoring systems. Proceedings of the Institution of Civil Engineers-Bridge Engineering, 2016: 126–38.
[5] Snæbjörnsson JT, Jakobsen JB, Cheynet E, Wang J. Full-scale monitoring of wind and suspension bridge response. IOP Conf Series 2017;276:012007. https://doi.org/10.1088/1757-899X/276/1/012007.
[6] Zheng H, Dang C, Gu S, Peng D, Chen Ke. A quantified self-adaptive filtering method: effective IMFs selection based on CEEMD. Meas Sci Technol 2018;29(8):085701. https://doi.org/10.1088/1361-6501/aac990.
[7] Shao Y, Miao C, Li B, Wu Q. Simultaneous de-noising and enhancement method for long-span bridge health monitoring data based on empirical mode decomposition and fractal conservation law. Meas Sci Technol 2019;30(6):065103. https://doi.org/10.1088/1361-6501/ab078c.
[8] Yang YB, Yang JP. State-of-the-art review on modal identification and damage detection of bridges by moving test vehicles. Int J Struct Stab Dyn 2018;18(02):1850025. https://doi.org/10.1142/S0219455418500256.
[9] Yang Y, Wang Z-L, Shi K, et al. State-of-the-art of the vehicle-based methods for detecting the various properties of highway bridges and railway tracks. Int J Struct Stab Dyn 2020. 2041004.
[10] Greco F, Lonetti P, Pascuzzo A. A moving mesh FE methodology for vehicle–bridge interaction modeling. Mech Adv Mater Struct 2020;27(14):1256–68.
[11] Sadeghi Eshkevari S, Matarazzo TJ, Pakzad SN. Simplified vehicle–bridge interaction for medium to long-span bridges subject to random traffic load. J Civil Struct Health Monit 2020;10(4):693–707.

[12] Frýba L. Vibration of solids and structures under moving loads. 1st ed. Springer Science & Business Media; 2013.
[13] Lou P. A vehicle-track-bridge interaction element considering vehicle's pitching effect. Finite Elem Anal Des 2005;41(4):397–427.
[14] Kwasniewski L, Li H, Wekezer J, Malachowski J. Finite element analysis of vehicle–bridge interaction. Finite Elem Anal Des 2006;42(11):950–9.
[15] Bathe K-J, Wilson EL. Numerical methods in finite element analysis. Prentice-Hall; 1976.
[16] Dokainish MA, Subbaraj K. A survey of direct time-integration methods in computational structural dynamics—I. Explicit methods. Comput Struct 1989;32 (6):1371–86.
[17] Zhong W, Williams F. A precise time step integration method. Proc Instit Mech Eng, Part C: J Mech Eng Sci, 1994, 208(6): 427–30.
[18] Brownjohn JMW, Pavic A. Experimental methods for estimating modal mass in footbridges using human-induced dynamic excitation. Eng Struct 2007;29(11): 2833–43.
[19] Ewins D. Modal testing: theory, practice and application. Baldock, Hertfordshire, England: Research Studies Press LTD.; 2000.
[20] Clough Ray W, Penzien J. Dynamics of structures. Computers & Structures, Inc; 1995.
[21] Ma L, Zhang W, Han WS, Liu JX. Determining the dynamic amplification factor of multi-span continuous box girder bridges in highways using vehicle-bridge interaction analyses. Eng Struct 2019;181:47–59.
[22] Henchi K, Fafard M, Talbot M, Dhatt G. An efficient algorithm for dynamic analysis of bridges under moving vehicles using a coupled modal and physical components approach. J Sound Vib 1998;212(4):663–83.
[23] Deng L. System identification of bridge and vehicle based on their coupled vibration. Louisiana State University; 2009.
[24] Park HS, Oh BK. Damage detection of building structures under ambient excitation through the analysis of the relationship between the modal participation ratio and story stiffness. J Sound Vib 2018;418:122–43.
[25] Seon Park H, Kim J, Oh BK. Model updating method for damage detection of building structures under ambient excitation using modal participation ratio. Measurement 2019;133:251–61.
[26] Zhang J, Gao Q, Tan SJ, Zhong WX. A precise integration method for solving coupled vehicle–track dynamics with nonlinear wheel–rail contact. J Sound Vib 2012;331(21):4763–73.
[27] Wan-Xie Z. On precise integration method. J Comput Appl Math 2004;163(1): 59–78.
[28] Tan S, Wu Z, Zhong W. Adaptive selection of parameters for precise computation of matrix exponential based on Padé approximation. Chinese J Theor Appl Mech 2009;41(6):961–6.
[29] Lin Y-H, Trethewey MW. Finite element analysis of elastic beams subjected to moving dynamic loads. J Sound Vib 1990;136(2):323–42.
[30] Bocian M, Brownjohn JMW, Racic V, Hester D, Quattrone A, Monnickendam R. A framework for experimental determination of localised vertical pedestrian forces on full-scale structures using wireless attitude and heading reference systems. J Sound Vib 2016;376:217–43.
[31] Brownjohn JMW, Bocian M, Hester D, Quattrone A, Hudson W, Moore D, et al. Footbridge system identification using wireless inertial measurement units for force and response measurements. J Sound Vib 2016;384:339–55.